WEI LI[1], ZHIWEN LYU[2], JIAN LIU[1], WEI LI[3], ZIQIANG SUN[4], YAN MA[4]
WEIMIN CHENG[2], XIANGJUN MENG[2], LIN XIN[2], XIKUI SUN[1]

PREPARATION OF SLAG-BASED FOAM CONCRETE BY CHEMICAL FOAMING FOR CO2 SEQUESTRATION

Carbon dioxide emissions are among the most influential causes of global warming, and the recovery, capture, and comprehensive utilization of CO_2 are the keys to carbon emissions reduction. High-porosity foam concrete was prepared using CaO as the alkali activator, and H_2O_2 as the foaming agent. Based on a single-factor experiment and response surface analysis, the best preparation conditions for foam concrete were obtained (water-to-cement ratio 0.4, alkali excitation dosage 10.73%, foaming agent dosage 8.26%). The porous material prepared under the optimal process conditions can achieve a CO_2 sequestration performance of 91.59 kg/m^3, and the actual sequestration capacity is consistent with the theoretical prediction value of 90.89 kg/m^3. Mechanistic analysis shows that the precarbonation hydration products of foam concrete are mainly C-S-H gel, $Ca(OH)_2$, and hydrotalcite-like compounds, which bond the slag particles together to form a three-dimensional spatially firmly connected structure. This study provides a reference for the application of alkaline solid waste materials in the field of carbon sequestration.

1. INTRODUCTION

Worldwide global warming mitigation has been prioritized by many countries. Climate change will cause hazardous secondary effects such as melting glaciers, more frequent natural disasters, and more virulent spread of infectious diseases, which will greatly affect human lives worldwide [1]. Reducing CO_2 emissions is a global goal set by the international community to combat climate change. The energy sector is a major

_____

[1]Shandong Energy Group Company Limited, Jinan 250101, Shandong.
[2]College of Safety and Environmental Engineering, Shandong University of Science and Technology, Qingdao 266590, China, corresponding author Z. Lyu, email address: 13598091558@163.com
[3]Shandong Energy Power Group Company Limited, Jinan 250014, Shandong.
[4]Shandong Luxi Power Generation Company Limited, Jining 272000, Shandong.

source of greenhouse gases, and despite new developments and policies, the global energy system remains unsustainable [2]. Global energy demand is predicted to increase by 33% by 2035, while CO_2 emissions are also expected to increase dramatically [3]. Consequently, countries are beginning to research and develop carbon capture technologies to help mitigate the effects of increasing CO_2 emissions. Domestic and international methods for capturing CO_2 have been reported extensively before, such as absorption, adsorption, membrane separation, hydrate-based separation techniques, and low-temperature distillation [4–6]. CO_2 captured by these methods can usually be used to produce high-value-added products such as ammonia, refrigerants, and fire-extinguishing gases [7].

However, current CO_2 utilization accounts for only 2% of emissions, and the CO_2 reduction effect is not significant. Carbon-negative methods are more prominent than carbon-neutral methods in the current CO_2 emissions scenario. CO_2 sequestration is an emerging post-combustion carbon capture technology using mineral carbonization, storing CO_2 permanently by reacting it with alkali metal oxides [8]. Xue et al. [9] collected and reviewed mineral carbon sequestration and available process routes for industrial waste, and concluded that mineral carbonation is the only known method for the permanent storage of CO_2. From a whole life cycle perspective, the use of CO_2 sequestration of industrial solid waste is a method with multiple potential applications and is gaining interest in the field [10]. Accelerated carbonization of alkaline wastes might offer a way to lower industrial net greenhouse gas emissions while serving as a trial run for wider adoption [11]. Carbonation curing is an economical way to use solid waste and produces a pH-neutral building material, making it ideal for the construction of artificial reefs for marine pastures and aquaculture farms [12, 13]. The results of a study by Jang et al. [14] showed that the concrete carbonation curing process can sequester CO_2 within a few hours to a few days, with a CO_2 sequestration rate of 24%. Pure cementitious materials (cement and concrete) can sequester CO_2 and the rate of CO_2 diffusion is the main controlling condition affecting the rate of early carbonation reactions in materials [15]. However, owing to the dense nature of concrete, the depth of carbonation is small; therefore, most of the components do not participate in the CO_2 reaction process. When considering the economic costs of implementing the technology and reducing the carbon footprint, it is essential to optimize the material components and preparation processes [9].

Wang et al. [16] introduced gypsum into the steel slag carbonation system, and accelerated the hydration of steel slag to generate calcite ($C_3A \cdot 3CaSO_4 \cdot 32H_2O$), subsequently reacted with CO_2 to generate monocarbonate, increasing the amount of CO_2 absorbed by steel slag. Li et al. [17] collected and compared current mineral carbonation methods and concluded that the energy consumption of the mineral carbonation reaction of mechanical pretreatment of raw materials is too high and difficult to apply industrially, so industrial wastes can be used as raw materials to reduce mineral carbonation costs. Therefore, the use of solid waste (fly ash, calcium carbide slag, blast furnace slag,

etc.) to prepare cementitious materials and solidify the materials to form porous structures through foaming technology can provide important support for the application of this technology in carbon sequestration. Park et al. [18] used stainless steel slag and fly ash as cementitious materials to sequester CO_2 and showed that foam concrete has a higher absorption rate of CO_2 than ordinary concrete.

Therefore, in this study, blast furnace slag (a by-product of blast furnace ironmaking, mainly composed of CaO, Al_2O_3, MgO, and SiO_2, which can react in an alkaline environment to form hydrated calcium silicate and hydrated calcium aluminate [19]) was chosen as the base material, and H_2O_2 was used as the foaming agent to prepare highly porous open-cell foam concrete in a calcium oxide alkali excitation system. Foamed concrete prepared by this method contains a large number of pores, which improves the circulation and diffusion rate of CO_2 within the foam concrete, thus improving the performance of the foam concrete in curing and sequestering CO_2. In this study, the effects of different factors on the sample preparation and CO_2 sequestration performance were investigated, and the materials were optimized by designing response surface experiments. Finally, the CO_2 sequestration performance and mechanism of the optimized materials will be investigated to support the application of solid waste-based materials in the field of CO_2 sequestration.

2. MATERIALS AND METHODS

Sample preparation. Granulated blast furnace slag using CaO as the alkali exciter, and H_2O_2 as the foaming agent was used to prepare the required foam concrete via chemical foaming. First, the pre-measured slag and the dry powdered foam stabilizer were poured into the mixing pot and stirred at low speed for 1 min, after which room temperature water was poured into the mixing pot and stirred at low speed for 1 min, and a CaO alkali exciter was added and stirred for 2 min. Afterward, the specimens were quickly poured into a pre-prepared 5×5×5 cm mold, left until the end of foaming, covered with a layer of cling film on the surface to prevent evaporation, left to stand for 1 day, and then de-molded and sent to the maintenance box in a plastic bag to be maintained until the specified age (3 days).

Experimental procedure. The experimental procedure for the carbonation of foam concrete samples is shown in Fig. 1. After the curing period, the square specimens of foam concrete were placed in a carbonation chamber, fed with high-purity CO_2 (>99% purity), and kept at constant pressure (0.1 MPa) in the chamber until the end of the sealing time (24 h). In this case, when studying the effect of single factors (water-to-ash ratio, CaO dosage, and H_2O_2 dosage) on the material properties, the samples with uncarbonized sequestered CO_2 were named not carbonized (NC) and carbonization completed (CC).
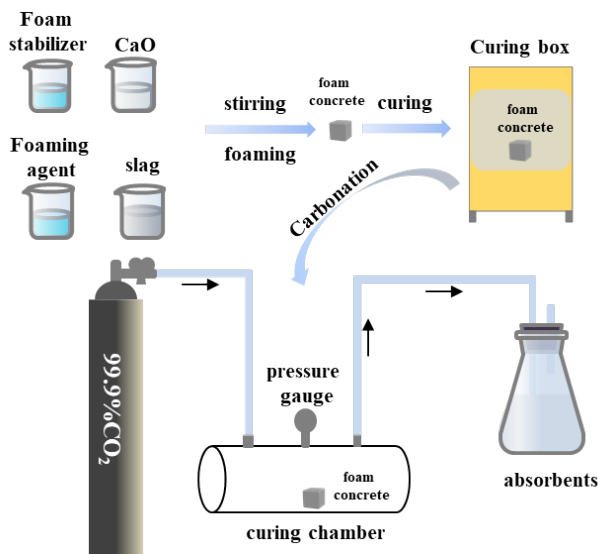
Fig. 1. Experimental flow chart

Analytical method. Changes in the surface, structural properties, and CO_2 sequestration were characterized using X-ray diffraction (XRD), Brunauer–Emmett–Teller (BET) specific surface area analysis, scanning electron microscopy (SEM), and thermogravimetric analysis (TGA).

Below 350 °C, it was mainly to remove free water and bound water. Below 520 °C, it mainly removed hydration products and unevaporated water in calcium hydroxide. The decomposition of calcium carbonate was predominant from 520 to 850 °C. The amount of carbon dioxide absorbed was calculated by [20]

$$CO_2 \ uptake = \frac{M_{520} - M_{850}}{M_d} \times 100\% \tag{1}$$

where M_{520}, M_{850}, and M_d are masse of the sample at 520, 850 °C, and after drying, respectively.

3. RESULTS AND DISCUSSION

3.1. RAW MATERIAL ANALYSIS

The granulated blast furnace slag (Rizhao slag) was obtained from Rizhao Steel Holding Group Limited. The chemical composition of the slag (Table 1) was determined using X-ray fluorescence (XRF) analysis. The slag was a white powder with a density

of 2.87 g/cm^3 and a fineness of approximately 397 m^2/kg. Figure 2 shows the XRD pattern of the slag. It showed a broad and diffuse diffraction peak spanning 2θ of 20–40°, indicating that the slag contained a phase dominated by a vitreous structure. During the production of slag from pig iron smelting, differences in the cooling rate of the slag and the immiscibility of the liquid phase result in the splitting of the vitreous structure, which results in a high hydration activity.

Table 1

Chemical composition of slag

Metal oxide	MgO	Al$_2$O$_3$	SiO$_2$	CaO	TiO$_2$	SO$_3$	Na$_2$O	MnO
Content [%]	7.27	14.14	24..09	47.73	2.59	1.62	0.41	0.70

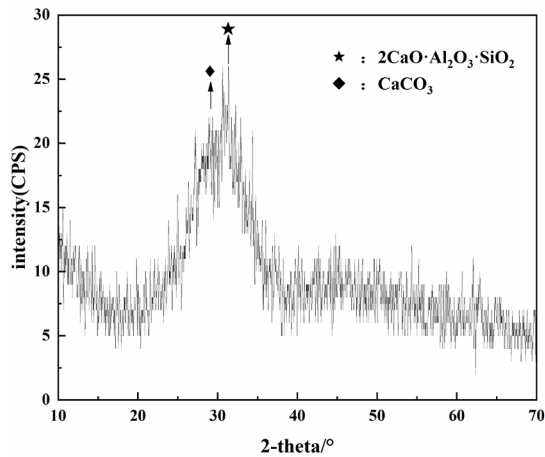Fig. 2. XRD pattern of slag

3.2. EFFECT OF PREPARATION CONDITIONS ON THE CARBON SEQUESTRATION PROPERTIES OF THE MATERIAL

3.2.1. EFFECT OF WATER TO ASH RATIO ON SAMPLE SEALING PERFORMANCE

The foam concrete was prepared according to the chemical foaming method, where the dosage of foam stabilizer was 0.8% of the slag mass, CaO was 5%, H$_2$O$_2$ was 10%, and the water-to-ash ratio was 0.4~0.8 (0.4, 0.5, 0.6, 0.7, and 0.8). The thermogravimetric curves before and after the carbonation of the samples with different water-to-ash ratios are shown in Fig. 3.

A significant weight loss occurs at 30–900 °C for each water-to-ash ratio before carbonization (Figs. 3a, b). The main focus was on the removal of free and bound water up to 350 °C, the removal of hydration products and unevaporated water from calcium hydroxide up to 520 °C, and the decomposition of calcium carbonate from 520 to 850 °C [21].
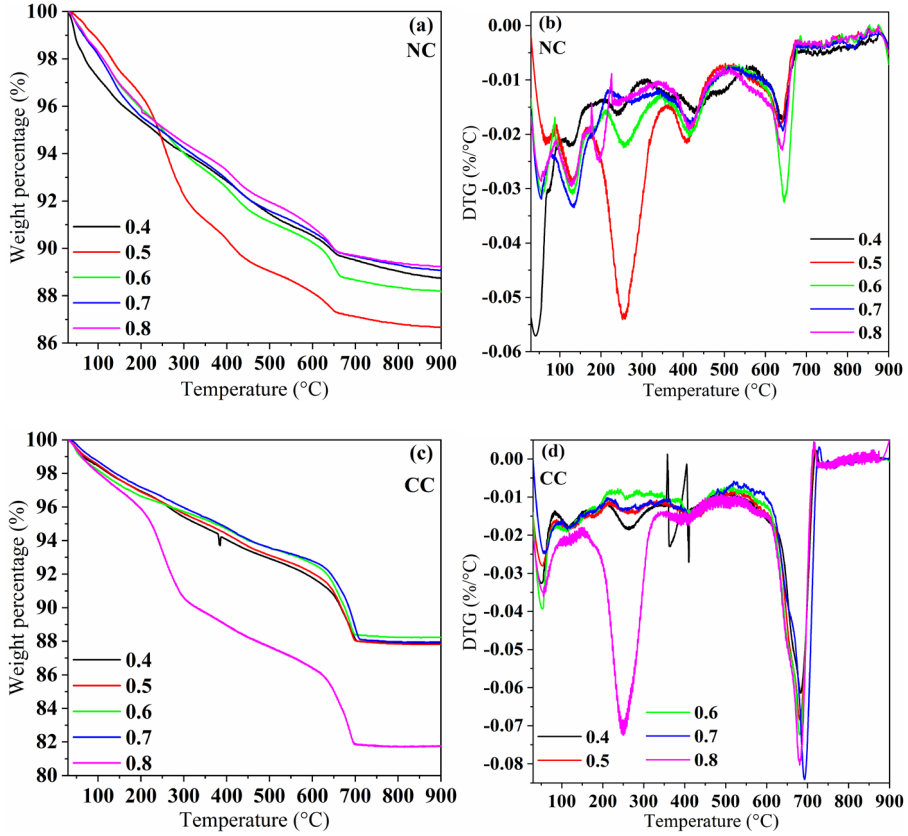
Fig. 3. TGA-DTG curves of the samples with different water-to-ash ratios:
a) TGA curve of the sample before carbonization, b) DTG curve of the sample before carbonization,
c) TGA curve of the sample after carbonization, d) DTG curve of the sample after carbonization

The weight losses of the uncarbonated samples prepared with the five water-to-ash ratios were 11.27, 13.36, 11.84, 10.94, and 10.79% throughout the temperature interval, respectively. Rapid weight loss of the C-S-H gel was observed in all samples from 100 to 200 °C, and the characteristic peak of weight loss of the hydrotalcite (Ht) phase, another important hydration product, appeared in the range of 200–350 °C. The peak of weight loss of $Ca(OH)_2$ was detected in the range of 350–500 °C. The temperature range of 500–900 °C was the peak of carbonate decomposition, with weight losses of 2.68, 2.49, 3.06, 2.52, and 2.79% for the five samples, respectively, which mainly originated from the carbonate contained in the specimens and the carbonation of $Ca(OH)_2$ during the preparation process [22]. As shown in Figs. 3c, d, the total weight losses of the five carbonized samples were 12.11, 12.18, 11.77, 12.05, and 18.22%, respectively. Unlike Fig. 3a, the weight loss of the samples increased significantly in the 500–900 °C range, mainly because of the decomposition of $CaCO_3$ formed after sequestering CO_2 in the

samples, with carbonate weight losses of 5.49, 5.84, 5.87, 6.24, and 7.02% for the five samples, respectively. Unlike the DTG curves in Fig. 3b, the weight loss rates of the C-S-H gel, Ht, and $Ca(OH)_2$ were all lower, implying that each hydration product effectively absorbed CO_2 during carbonation and converted it to $CaCO_3$-dominated carbonate. At a water-to-ash ratio of 0.8, the carbonate weight loss was reduced, indicating that the water-to-ash ratio was too large and not conducive to curing CO_2 in the sample.

The dry densities of uncarbonized samples and their CO_2 sequestration were investigated at different water-to-ash ratios. The dry densities of the five water-to-ash samples were 621.64, 587.74, 569.71, 480.01, and 417.02 kg/m^3, respectively. In other words, the dry density gradually decreased as the water-to-ash ratio increased. The corresponding CO_2 sequestration amounts for the five samples were 17.77, 19.66, 16.17, 17.85, and 17.61 kg/m^3, respectively, showing an overall increasing and then decreasing trend. At low water-to-ash ratios (0.4), there is less moisture, higher dry density, lower reaction of the cementitious material, fewer hydration products, less CO_2 dissolved to form CO_3^{2-}, and ultimately lower sequestration. Ht is formed at a water-to-ash ratio of 0.5. Ht ($[Mg_6Al_2(OH)_{16}CO_3]\cdot4H_2O$) has an octahedral anionic lamellar structure with cations and interlayer anions and exchangeable bimetallic hydroxides on the lamellae, which have good CO_2 adsorption capacity [23], leading to increased sequestration. When the water-cement ratio is 0.7, the hydration reaction proceeds to produce more hydration products, and during the curing process of foam concrete, the pore water inside the slurry evaporates and leaves pores to form connecting holes, increasing the rate of CO_2 diffusion, thus increasing the sequestration amount. When the water-to-ash ratio increased to 0.8, the CO_2 sequestration performance decreased again, likely due to the strong fluidity of the slurry and the ease with which the pores broke up inside the concrete, resulting in poor material pore formation. Although more hydration products were generated, the diffusion of CO_2 gas within the foam concrete was inhibited, resulting in lower sequestration.

3.2.2. EFFECT OF CaO DOSAGE ON SAMPLE SEALING PERFORMANCE

The water-to-ash ratio was chosen as 0.5, the dosages of foam stabilizer and H_2O_2 were 0.8 and 10% of the slag mass, respectively, and the dosages of CaO were 5, 7, 9, 11, and 13%, respectively. The thermogravimetric curves of the samples before and after carbonization are shown in Fig. 4.

All samples showed significant weight loss from 30 to 900 °C (Fig. 4a, b). The weight losses of the uncarbonated samples prepared with the five CaO dosages were 13.35, 13.16, 13.65, 12.68, and 12.42% throughout the temperature interval, respectively. At 13% CaO, the Ht phase and $Ca(OH)_2$ content of the hydration products in the specimen were reduced compared to other CaO dosages, indicating that too high CaO dosage may limit the production of the hydration products. As can be seen in Figs. 4c, d, the weight losses of the five post-carbonization samples were 12.18, 13.66, 14.33, 14.63, and 16.27%, respec-

tively, throughout the temperature interval. Unlike the DTG curve in Fig. 4b, the temperature interval below 500 °C in the carbonated samples was flat, and the carbonate weight losses for the five samples were 5.84, 7.76, 9.51, 10.23, and 10.03%, respectively, which were significantly greater than those of the uncarbonated samples.
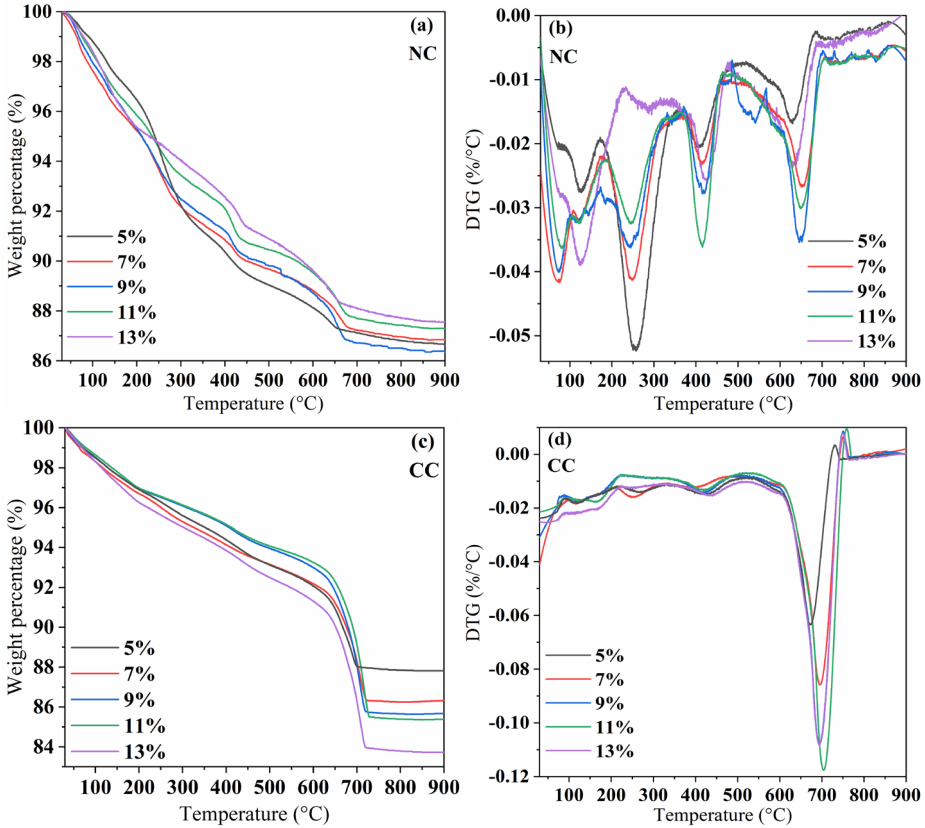

Fig. 4. TGA-DTG curves of the samples with different CaO dosages:
a) TGA curve of the sample before carbonization, b) DTG curve of the sample before carbonization,
c) TGA curve of the sample after carbonization, d) DTG curve of the sample after carbonization)

The dry density of the uncarbonized samples and their CO_2 sequestration were investigated at different CaO dosages. The dry densities of the five samples were 527.74, 600.81, 710.69, 809.43, and 850.01 kg/m^3, respectively. The dry density gradually increased with an increase in the CaO dosage. The corresponding CO_2 sequestration amounts for the five samples are 17.65, 28.25, 40.51, 53.98, and 52.06 kg/m^3 respectively. This is because, as the amount of exciter increases, it tends to break the covalent bonds of Ca-O, Mg-O, Si-O-Si, Al-O-Al, and Al-O-Si in the vitreous structure of the slag, forming hydration products and leading to an increase in the dry density of the

sample [24]. When the CaO dosage (13%) was too high, a large amount of Ca^{2+} was dissolved from the calcium oxide, and the resulting hydration products covered the surface of the slag, limiting the production of internal hydration products and ultimately leading to no significant increase in dry density and a reduction in sequestration.

3.2.3. EFFECT OF H_2O_2 DOPING ON THE SEALING PERFORMANCE OF THE SAMPLES

A water-to-ash ratio of 0.5, foam stabilizer dosage of 0.8 wt. %, and CaO dosage of 11% were chosen to investigate the effect of H_2O_2 dosage (6, 8, 10, and 12%) on the sealing performance of the samples. The thermogravimetric curves of the samples before and after carbonization with different amounts of H_2O_2 are shown in Fig. 5.
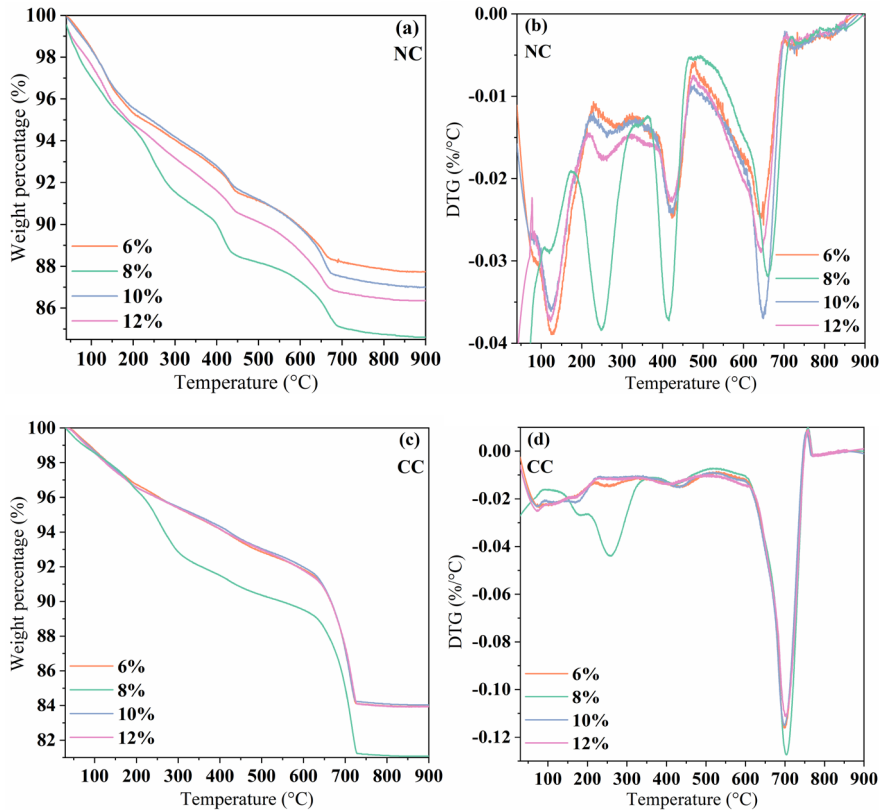

Fig. 5. TGA-DTG curves of the samples at different H_2O_2 dosages:
a) TGA curve of the sample before carbonization, b) DTG curve of the sample before carbonization,
c) TGA curve of the sample after carbonization, d) DTG curve of the sample after carbonization

As can be seen in Figs. 5a, b, the total weight losses of the uncarbonated samples prepared with the four H_2O_2 dosages were 12.25, 15.39, 12.71, and 13.64%, respectively. The Ht phase and $Ca(OH)_2$ weight loss of the hydration products in the specimens

increased significantly when the H_2O_2 dosage was 8%. This is because too high dosage of H_2O_2 (10 and 12%) may limit the production of hydration products resulting in lower weight loss for both. In the carbonate weight-loss interval, the weight losses of the four uncarbonated samples were 3.63, 4.02, 3.47, and 4.09%, respectively. As shown in Figs. 5c, d, the weight losses of the four carbonized samples were 16.06, 18.92, 14.62, and 16.05%, respectively. Unlike the DTG curve in Fig. 5(b), there is still an Ht phase that is not involved in the carbonation reaction at 8% H_2O_2 dosage. The samples with 6, 10, and 12% H_2O_2 exhibited a flat profile in the temperature range of up to 500°C. The weight losses of the carbonized samples were 10.41, 11.27, 10.03, and 10.55%, respectively, which were significantly greater than those of the uncarbonized samples.

The dry densities of the four H_2O_2 dosage samples were 1204.44, 1100.02, 820.05, and 691.18 kg/m^3, respectively. They gradually decreased with increasing H_2O_2 dosage. AS the H_2O_2 content increases, so does the production of oxygen, resulting in an increasing number of air bubbles in the fresh slurry and ultimately a smaller dry density. The amount of CO_2 sequestered was 69.85, 53.74, and 44.59 kg/m^3 at 6, 10 and 12% H_2O_2 respectively. In contrast, at 8% H_2O_2, the reaction conditions were favorable for the production of the hydration product Ht phase, resulting in the largest CO_2 sequestration of 80.74 kg/m^3.

3.3. OPTIMISATION RESULTS FOR FOAM CONCRETE CONDITIONS

Based on the response surface Box–Behnken experimental design theory combined with the results of the single-factor experiments, three main factors affecting CO_2 sequestration (Q_e) were selected: the water to ash ratio (A), CaO dosage (B), and H_2O_2 dosage (C). These factors were combined, and 3 factors and 3 levels were determined for response surface analysis, the experimental factors and level codes are shown in Table 2.

Table 2

Actual variables of the BBD
design and their level values

Response variable	Level		
	−1	0	1
A	0.40	0.50	0.60
B, %	10	11	12
C, %	7	8	9

Design-Expert software (version 8.0) was used to design and prepare Box–Behnken response surface experiments for carbon dioxide sequestration in foam concrete; the experimental results are shown in Table 3. As shown in Table 3, the difference between the actual and predicted values for the 17 sets of experiments was small. The highest

CO_2 sequestration was 80.74 kg/m^3 in Group 15 and 29.22 kg/m^3 in Group 14. The statistics and analysis of the results of the 17 sets of experiments on the Box–Behnken response surface enabled the derivation of the extent to which individual factors influenced the response values and the magnitude of the interactions between the factors.

Table 3

Box–Behnken test design and results

Run	Factor			Response	
	A	B [%]	C [%]	Q_e [kg/m^3]	
				Actual value	Predicted value
1	0.40	10.00	8.00	74.83	75.85
2	0.60	11.00	7.00	71.16	71.25
3	0.50	11.00	8.00	80.66	79.89
4	0.50	12.00	7.00	52.52	53.44
5	0.50	11.00	8.00	80.11	79.89
6	0.60	12.00	8.00	55.99	54.96
7	0.40	11.00	9.00	79.93	79.84
8	0.40	11.00	7.00	69.01	67.64
9	0.50	10.00	9.00	42.07	41.14
10	0.50	10.00	7.00	40.86	41.19
11	0.50	11.00	8.00	78.26	79.89
12	0.50	11.00	8.00	79.66	79.89
13	0.60	11.00	9.00	33.08	34.44
14	0.50	12.00	9.00	29.22	28.89
15	0.50	11.00	8.00	80.74	79.89
16	0.40	12.00	8.00	53.41	53.82
17	0.60	10.00	8.00	33.36	32.93

The final quantitative relationship between the three response variables and CO_2 sequestration represents Eq. (2) elaborated based on the Design-Expert software (version 8.0) to fit the regressions for each factor. The positive and negative signs in Eq. (2) denote synergistic and antagonistic effects, respectively.

$$Q_e = 79.89 - 10.45A + 5.706 \times 10^{-4}B - 6.15C + 11.02AB$$
$$-12.25AC - 6.13BC - 1.68A^2 - 23.81B^2 - 14.91C^2 \tag{2}$$

Analysis of variance (ANOVA) was also used to explore the significance and fitness of the fitted second-order model. Table 4 presents the results of the analysis of variance for the model variables. The F-value of the model (379.67) and the corresponding P-value (<0.0001) indicate that the model is significant and that there is only a 0.01% probability that the F-value of the model is due to noise [25]. The linear relationship

between these factors and the amount of CO_2 sequestered was significant, and the experimental model was reliable. The P-value of 0.1832 for the misfit term was much greater than 0.05, indicating that the fitted second-order model can be applied to this experiment [26]. The model can be considered plausible when the ratio of the model signal to noise is greater than 4 [27]. The signal-to-noise ratio of this model was 50.392, indicating that the fitted model accurately replicates the experimental conditions. The coefficient of variation (CV, %) reflects the reproducibility of the second-order model, and the CV for this experiment was 2.17% less than 10%, indicating that the expected model has good confidence. The correlation coefficient R^2 of the regression equation was 0.9980, indicating that the fitted regression model could express 99.80% of the response to the variables. R^2 greater than 0.8 indicates that the model fits well with the measured data. The difference between R^2 (0.9980) and the corrected R^2 (0.9953) implies the presence of a non-significant term in the model. The difference between the two is 0.0027, less than 0.2, indicating good confidence in the model [28]. Based on the above ANOVA results, it can be concluded that the fitted model can be used to simulate the effects of the water-to-ash ratio, CaO dosage, and H_2O_2 dosage on the amount of CO_2 sequestered.

Table 4

Model of variance results for the quadratic model

Source of variance	Quadratic sum	Degree of freedom	Mean square	F-value	P-value	Remarks
Model	5964.28	9	662.70	379.67	<0.0001	significant
A	873.19	1	873.19	500.26	<0.0001	
B	2.605E–006	1	2.605E–006	1.492E–006	0.9991	
C	302.72	1	302.72	173.43	<0.0001	
AB	485.35	1	485.35	278.06	<0.0001	
AC	600.42	1	600.42	343.99	<0.0001	
BC	150.12	1	150.12	86.00	<0.0001	
A^2	11.94	1	11.94	6.84	0.0347	
B^2	2387.19	1	2387.19	1367.65	<0.0001	
C^2	935.99	1	935.99	536.24	<0.0001	
Residuals	12.22	7	1.75			
Loss of proposed items	8.15	3	2.72	2.67	0.1832	not significant
Standard deviation	1.32	1.32	1.32	0.9980		
Average value	60.87	60.87	60.87	0.9953		
CV, %	2.17	2.17	2.17	0.9771		
			1.32	50.392		

To further investigate the effect of the interaction between the response variables on CO_2 sequestration, 3D response surface and contour plots of the experimental model were obtained using Design Expert (Fig. 6).

For a given amount of blowing agent, the sequestration content gradually decreased as the water-to-ash ratio increased (Fig. 6a). As the CaO alkali exciter dosage increased, the sequestration content first increased and then decreased, indicating that an optimum alkali exciter dosage exists in the range of 10–12%. The contour plot in Fig. 6b is elliptical, indicating a clear interaction between these two factors. Both factors had a significant effect on the experimental results, but that of the amount of alkali exciter was higher. From Figure 6c, it can be seen that with a certain amount of CaO, the response value gradually decreases as the water-to-ash ratio increases. However, as the amount of H_2O_2 increased, the response values showed a trend of increasing and then decreasing.
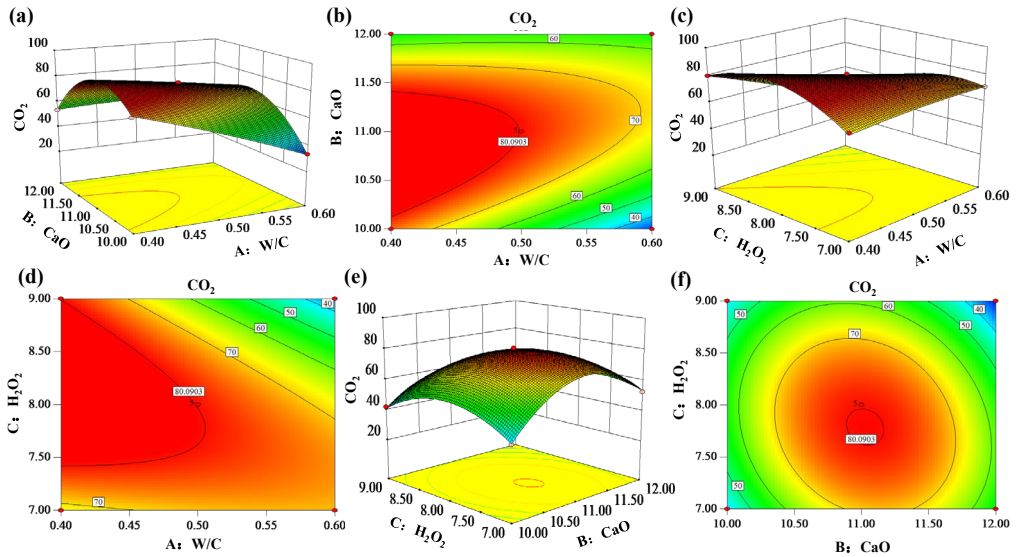

Fig. 6. Response surfaces (a) and contour plots (b) for the interaction between water-ash ratio and CaO dosage on CO_2 sequestration, response surfaces, and (c) contour plots for the interaction between water-ash ratio and H_2O_2 dosage on CO_2 sequestration (d), response surface (e) and contour plot for the interaction between CaO and H_2O_2 on CO_2 sequestration (f)

In summary, both the H_2O_2 dosage and the water-to-ash ratio affect the CO_2 sequestration content of the samples. The elliptical shape of the contour plot in Fig. 6d indicates that the interaction between the two factors, H_2O_2 dosage, and water-to-ash ratio, is significant; however, the H_2O_2 dosage has a higher influence. From Figure 6e, it can be seen that for a given water-to-ash ratio, the amount of sequestration increases and then decreases as the amount of alkali exciter increases, indicating that there is an

optimum amount of alkali exciter within the chosen range. As the amount of blowing agent increased, the amount of sequestration increased and then decreased, indicating that there was an optimum amount of blowing agent within the chosen range. The contour plot in Fig. 6f is elliptical, indicating a significant interaction between these two factors.

A second-order model was fitted to this study using the Design Expert software (version 8.0) to predict the optimal values and obtain the best combination of conditions for the three response variables and corresponding CO_2 sequestration amounts. Table 5 shows the results of the process optimization. The best preparation conditions were determined as follows: water-to-ash ratio of 0.4, alkali excitation dosage of 10.73%, and foaming agent dosage of 8.26%.

T a b l e   5

Process optimization results

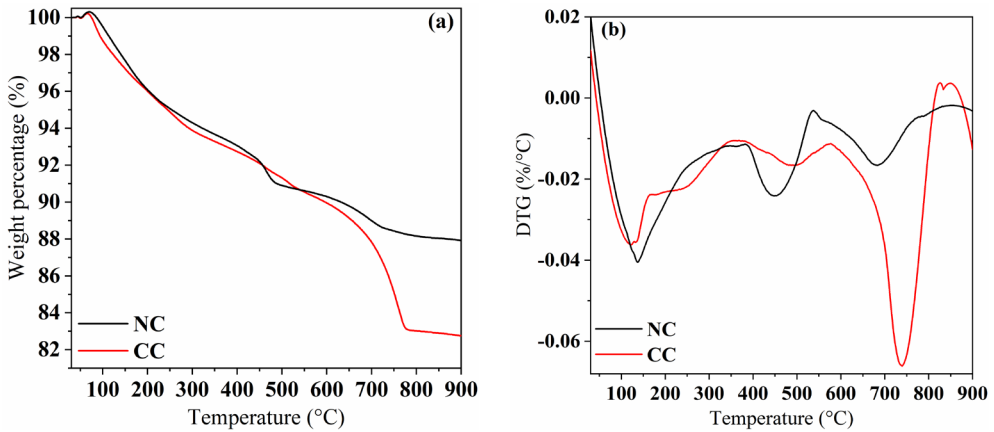| A	B	C	CO_2 sequestration
	10.73	8.26	90.8968
	10.73	8.25	90.8954
0.40	10.72	8.26	90.8932
	10.74	8.28	90.8917

Fig. 7. TGA-DTG diagram of the highest sequestered volume of foam concrete
a) wt. % loss, b) DTG curve

Figure 7 shows the thermogravimetric plot of the foam concrete for the highest sequestration volume. To verify the optimal response values predicted by the fitted model, foam concrete was prepared under optimal process conditions, and CO_2 sequestration experiments were conducted on the optimal group. To reduce this error, three sets of experiments were conducted and the average of the results was 90.91 kg/m³. The highest

sequestered amount of foam concrete had a dry density of 1382.93 kg/m^3, a carbonate weight loss of 6.62%, and a CO_2 sequestration of 91.59 kg/m^3.

3.4. INVESTIGATION OF THE CO_2 SEQUESTRATION MECHANISM

The N$_2$ adsorption-desorption isotherms and pore size distributions of the NC and CC samples are shown in Fig. 8. The N$_2$ adsorption capacity of the CC sample decreased significantly compared to that of the NC sample. The adsorption performance of the sample decreased after carbonization, probably due to the reduction of the pore size and thus adsorption capacity. As shown in Fig. 8b, the pore size distribution of the optimal system before carbonization was between 2 and 33 nm, whereas after carbonization it was between 2 and 26 nm. The samples were predominantly mesoporous before and after carbonization, indicating that the carbonization reaction did not change the pore type of the samples but only their sizes. The NC samples showed double peaks at 2–5 nm and 5–8 nm, while the highest peak of the CC samples appeared at 6–10 nm, and the top of the peak was gentler. It seems that most of the pore size range of the carbonized sample was concentrated in the gel pores, and the proportion of gel pores was significantly increased [29].
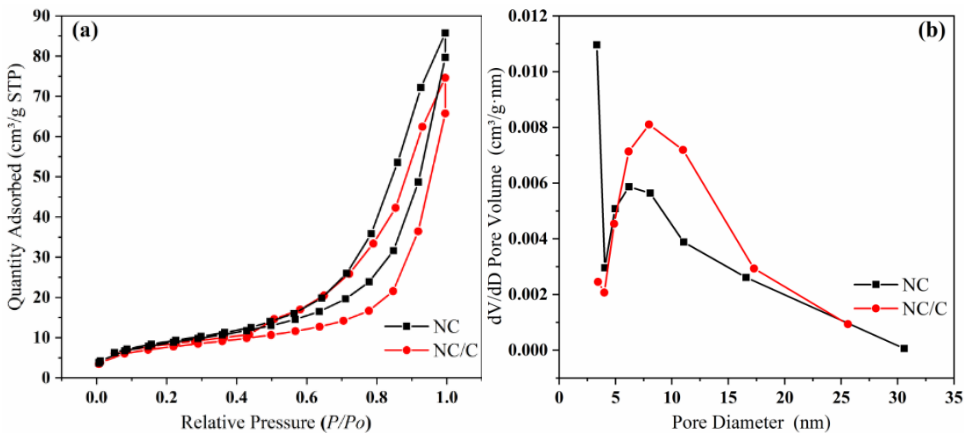

Fig. 8. N$_2$ adsorption-desorption isotherms (a) and comparative pore size distribution (b) for NC and CC samples

T a b l e 6

NC and CC specific surface areas and pore structure

Sample	BET specific surface [m^2/g]	Pore volume [cm^3/g]	Average pore diameter [nm]
NC	46.319	0.115	10.017
CC	45.996	0.112	9.756

As shown in Table 6, the pore volume, pore size, and specific surface area of the CC samples were lower than those of the NC samples. This may be due to the reaction of hydration products (C-S-H gel, Ht phase, $Ca(OH)_2$) with CO_2 during the carbonation reaction to produce structurally stable $CaCO_3$ that blocks the pores, thus reducing the pore volume, average pore size, and specific surface area [30].
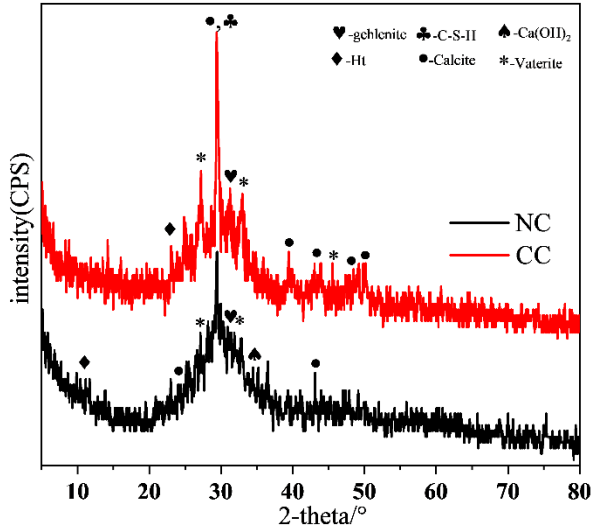

Fig. 9. XRD plots of NC and CC samples

The XRD patterns of the samples before and after carbonization are shown in Fig. 9. The diffraction peaks of the calcium-aluminum xanthite phase were detected at 2θ of 31.29° before and after carbonization, which is probably due to the phase not being hydrated and stable in its crystalline state.

At $2\theta = 29.5°$, the main hydration product of alkali-excited slag-based gelling materials is C-S-H gel. The Ht phase is also an important hydration product during alkali-excited slag hydration and is dominated by a double layer of metal hydroxides consisting of Ca^{2+} (or Mg^{2+}) and Al^{3+}. In the XRD pattern, the diffraction peaks of the Ht phase are mainly located at 2θ of 10.9° and 23.3° [22]. The characteristic peaks of the NC samples at $2\theta = 24.8°$ and 43.9° are characteristic diffraction peaks of vaterite-type $CaCO_3$, which may be due to the formation of amorphous or low-crystalline vaterite-type carbonates as a result of the carbonation of the C-S-H gel during the conservation process [12]. In addition, the presence of C-S-H gel alongside $CaCO_3$ shows that slag carbonation and hydration occur concurrently. Unlike NC, the intensity of the $CaCO_3$ diffraction peak at 29.41° was much higher in the CC sample, and new diffraction peaks of $CaCO_3$ appeared at approximately $2\theta = 39.41°$, 47.46°, and 48.21°. The reaction of calcium ions with carbonate ions generated by dissolving CO_2 in the curing chamber,

promoted the production of $CaCO_3$ and further demonstrated the ability of this research to effectively carbonate and sequester CO_2.

The microscopic morphology of the samples before and after carbonization was characterized using SEM, and the results are shown in Fig. 10.
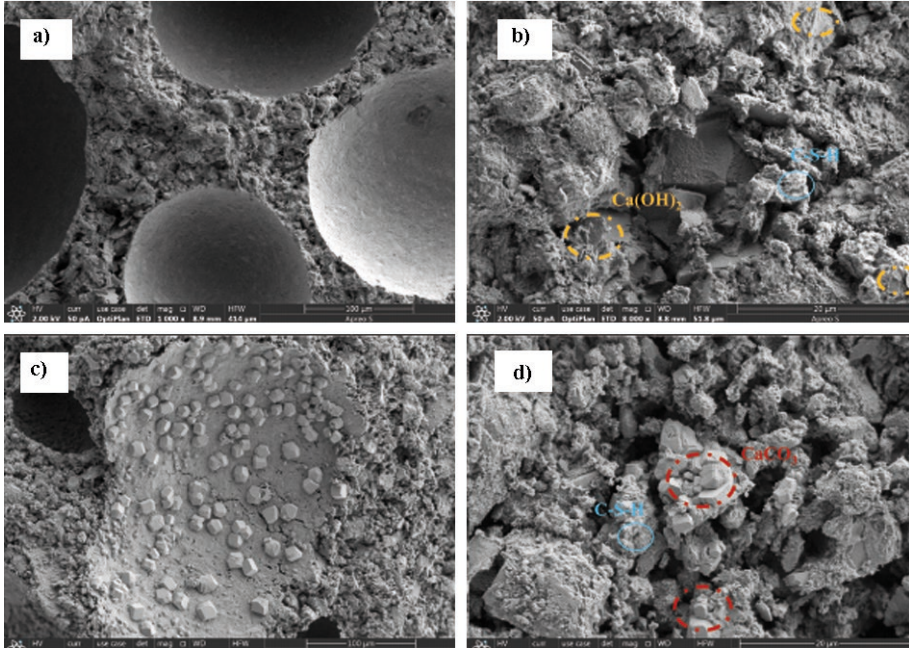

Fig. 10. SEM images of the samples of the optimum system:
a) NC, b) NC magnified 15 000×, c) CC, d) CC magnified 15 000×

Figure 10a shows a cross-section of the pore wall for the optimal system NC. It can be observed that the surface of the sample before carbonization is dense and that the internal pore walls are smooth and free of particles. As can be seen in Fig. 10b, the surface of the slag particles is wrapped by a large number of fibrous C-S-H gel, and the originally dispersed slag forms a compact whole. This is due to the hydration reaction that takes place and the hydration products joining the slag particles together, thus form-ing a three-dimensional tightly bound structure. During the hydration reaction of the slag, flakes of irregularly shaped hydration product $Ca(OH)_2$ can be observed, which coincides with the XRD spectrum. As can be seen from Fig. 10c, the stomata in the CC sample are lined with many small hexahedral-shaped particles. During the carbonation process, the foam concrete absorbs CO_2, and CO_3^{2-} ions formed by hydrolysis occurs in chemical bonding with Ca^{2+} in the system, nucleating $CaCO_3$ crystals by ion collisions and settling on the surface of the pore wall. The surface of the slag particles dissolves under the action of the alkali exciter, and the dissolved ions react around the slag to

wrap around the slag particles (Fig. 10d). Meanwhile, in the fibrous C-S-H gel, the flaky $Ca(OH)_2$ disappears, and the carbonation product ($CaCO_3$) is formed after the carbonation reaction and settles on the surface of the foam concrete pore wall.

4. CONCLUSIONS

The effects of water-cement ratio, CaO dosage, and H_2O_2 dosage on CO_2 sequestration in cured foam concrete were investigated. Based on single-factor experiments combined with response surface analysis, the preparation process of CaO-excited slag-based foam concrete for CO_2 sequestration was optimized and the mechanism of CO_2 sequestration by foam concrete was demonstrated. The following conclusions were drawn.

• Three single factors, the water-to-ash ratio, CaO dosage, and H_2O_2 dosage, were measured by TGA to determine the amount of CO_2 sequestered and where the water-to-ash ratio was too low or too high for CO_2 sequestration to occur. CO_2 sequestration increases as the CaO dosage increases, whereas a CaO dosage that is too high (13%) limits the production of internal hydration products and ultimately leads to lower sequestration. A dosage of 8% H_2O_2 favored the generation of the hydration product Ht phase, resulting in a maximum CO_2 sequestration of 80.74 kg/m^3.

• The regression equations of the three response variables and CO_2 sequestration were determined based on single-factor experiments combined with response surface analysis. The correlation coefficient R^2 was 0.9980, indicating that the model fitted well with the measured data. The optimum conditions for the preparation of foam concrete were obtained through response surface experiments: water-to-ash ratio of 0.4, alkali excitation dosage of 10.73%, and foaming agent dosage of 8.26%. The theoretically predicted value of CO_2 storage under optimal process conditions is 90.89 kg/m^3 and the actual value is 91.59 kg/m^3.

• The hydration products of foam concrete before carbonation were mainly C-S-H gel, $Ca(OH)_2$, and Ht. After the carbonation reaction, the specific surface area, pore volume, and pore size of the samples decreased. This was probably due to the continuous carbonation of the hydration products to produce $CaCO_3$-based carbonates to fill the pores. During carbonation, Ca^{2+} reacts with CO_3^{2-} in the solution and settles on the surface of the foam concrete pore walls. As the $CaCO_3$ attached to the surface of the reaction phase continues to increase, the pores are blocked and CO_2 is prevented from entering the interior of the foam concrete, leading to the end of the reaction.

REFERENCES

[1] ZHAO B., SUN L., QIN L., *Optimization of China's provincial carbon emission transfer structure under the dual constraints of economic development and emission reduction goals*, Environ. Sci. Pollut. R., 2022, 29, 50335–50351. DOI: 10.1007/s11356-022-19288-7.

[2] TAMILSELVI DANANJAYAN R.R., KANDASAMY P., ANDIMUTHU R., *Direct mineral carbonation of coal fly ash for CO_2 sequestration*, J. Clean. Prod., 2016, 112, 4173–4182. DOI: 10.1016/j.jclepro.2015.05.145.

[3] GAO P., YUE S., CHEN H., *Carbon emission efficiency of China's industry sectors: From the perspective of embodied carbon emissions*, J. Clean. Prod., 2021, 283. DOI: 10.1016/j.jclepro.2020.124655.

[4] LIU Y., WU J., ZHANG C., CHEN Y., XIONG M., SHI R., LIN X., YU X., *Thermodynamic and kinetic study of CO2 adsorption/desorptionon amine-functionalized sorbents*, Indian J. Chem. Techn., 2019, 26 (6), 473–482. DOI: 10.56042/ijct.v26i6.21111.

[5] LEE S., BINNS M., KIM J., *Automated process design and optimization of membrane-based CO_2 capture for a coal-based power plant*, J. Membr. Sci., 2018, 563, 820–834. DOI: 10.1016/j.memsci.2018.06.057.

[6] ZHANG W., JIN X., TU W., MA Q., MAO M., CUI C., *Development of MEA-based CO_2 phase change absorbent*, Appl. Energ., 2017, 195, 316–323. DOI: 10.1016/j.apenergy.2017.03.050.

[7] LEUNG D.Y.C., CARAMANNA G., MAROTO-VALER M.M., *An overview of current status of carbon dioxide capture and storage technologies*, Renew. Sust. Energ. Rev., 2014, 39, 426–443. DOI: 10.1016/j.rser.2014.07.093.

[8] MO L., ZHANG F., PANESAR D K., DENG M., *Development of low-carbon cementitious materials via carbonating Portland cement-fly ash-magnesia blends under various curing scenarios: a comparative study*, J. Clean. Prod., 2017, 163, 252–261. DOI: 10.1016/j.jclepro.2016.01.066.

[9] XUE Q., ZHANG L., MEI K., WANG L., WANG Y., LI X., CHENG X., LIU H., *Evolution of structural and mechanical properties of concrete exposed to high concentration CO_2*, Const. Build. Mater., 2022, 343, 128077. DOI: 10.1016/j.conbuildmat.2022.128077.

[10] PORTILLO E., ALONSO-FARINAS B., VEGA F., CANO M., NAVARRETE B., *Alternatives for oxygen-selective membrane systems and their integration into the oxy-fuel combustion process: A review*, Sep. Purif. Technol., 2019, 229, 115708. DOI: 10.1016/j.seppur.2019.115708.

[11] POWER I.M., HARRISON A.L., DIPPLE G.M., WILSON S.A., KELEMEN P.B., HITCH M., SOUTHAM G., *Carbon mineralization: From natural analogues to engineered systems*, 2013, 77. 305–360. DOI: 10.2138/rmg.2013.77.9.

[12] LI J., ZHAO S., SONG X., NI W., MAO S., DU H., ZHU S., JIANG F., ZENG H., DENG X., HITCH M., *Carbonation curing on magnetically separated steel slag for the preparation of artificial reefs*, Materials, 2022, 15 (6), 2055. DOI: 10.3390/ma15062055.

[13] BA H., LI J., NI W., LI Y., JU Y., ZHAO B., WEN G., HITCH M., *Effect of calcium to silicon ratio on the microstructure of hydrated calcium silicate gels prepared under medium alkalinity*, Constr. Build. Mater., 2023, 379, 131240. DOI: 10.1016/j.conbuildmat.2023.131240.

[14] JANG J.G., KIM G.M., KIM H.J., LEE H.K., *Review on recent advances in CO_2 utilization and sequestration technologies in cement-based materials*, Constr. Build. Mater., 2016, 127, 762–773. DOI: 10.1016/j.conbuildmat.2016.10.017.

[15] QIN L., GAO X., *Recycling of waste autoclaved aerated concrete powder in Portland cement by accelerated carbonation*, Waste Manage., 2019, 89, 254–264. DOI: 10.1016/j.wasman.2019.04.018.

[16] WANG X., NI W., LI J., ZHANG S., HITCH M., PASCUAL R., *Carbonation of steel slag and gypsum for building materials and associated reaction mechanisms*, Cem. Conc. Res., 2019, 125, 105893. DOI: 10.1016/j.cemconres.2019.105893.

[17] LI J., HITCH M., *Mechanical activation of magnesium silicates for mineral carbonation. A review*, Miner. Eng., 2018, 128, 69–83. DOI: 10.1016/j.mineng.2018.08.034.

[18] PARK B., CHOI Y.C., *Investigation of carbon-capture property of foam concrete using stainless steel AOD slag*, J. Clean. Prod., 2021, 288, 125621. DOI: 10.1016/j.jclepro.2020.125621.

[19] CORREA-SILVA M., MIRANDA T., ROUAINIA M., ARAUJO N., GLENDINNING S., CRISTELO N., *Geomechanical behaviour of a soft soil stabilised with alkali-activated blast-furnace slags*, J. Clean. Prod., 2020, 267, 122017. DOI: 10.1016/j.jclepro.2020.122017.

[20] TU Z., GUO M., POON C.S., SHI C., *Effects of limestone powder on $CaCO_3$ precipitation in CO_2 cured cement pastes*, Cem. Conc. Comp., 2016, 72, 9–16. DOI: 10.1016/j.cemconcomp.2016.05.019.

[21] ABDALQADER A.F., JIN F., AL-TABBAA A., *Characterisation of reactive magnesia and sodium carbonate-activated fly ash/slag paste blends*, Const. Build. Mater., 2015, 93, 506–513. DOI: 10.1016/j.conbuildmat.2015.06.015.

[22] DUAN W., LI G., WANG Z., WANG D., YU Q., ZHAN Y., *Highly efficient production of hydrotalcite-like compounds from blast furnace slag*, Appl. Clay Sci., 2022, 219, 106441. DOI: 10.1016/j.clay.2022.106441.

[23] ZHANG W., CHENG H., PENG S., LI D., GAO H., WANG D., *Performance and mechanisms of wastewater sludge conditioning with slag-based hydrotalcite-like minerals (Ca/Mg/Al-LDH)*, Water Res., 2020, 169, 115265. DOI: 10.1016/j.watres.2019.115265.

[24] MOZTAHIDA M., LEE D.S., *Photocatalytic degradation of methylene blue with P25/graphene/polyacrylamide hydrogels: Optimization using response surface methodology*, J. Hazard. Mater., 2020, 400, 123314. DOI: 10.1016/j.jhazmat.2020.123314.

[25] BAZRAFSHAN E., AL-MUSAWI T.J., SILVA M.F., PANAHI A.H., HAVANGI M., MOSTAFAPUR F.K., *Photocatalytic degradation of catechol using ZnO nanoparticles as catalyst: Optimizing the experimental parameters using the Box–Behnken statistical methodology and kinetic studies*, Microchem. J., 2019, 147, 643–653. DOI: 10.1016/j.microc.2019.03.078.

[26] RAHIMI B., JAFARI N., ABDOLAHNEJAD A., FARROKHZADEH H., EBRAHIMI A., *Application of efficient photocatalytic process using a novel $BiVO/TiO_2$-NaY zeolite composite for removal of acid orange 10 dye in aqueous solutions: Modeling by response surface methodology (RSM)*, J. Environ. Chem. Eng., 2019, 7 (4), 103253. DOI: 10.1016/j.jece.2019.103253.

[27] UMER M., TAHIR M., AZAM M.U., TASLEEM S., ABBAS T., MUHAMMAD A., *Synergistic effects of single/multiwalls carbon nanotubes in TiO_2 and process optimization using response surface methodology for photocatalytic H_2 evolution*, J. Environ. Chem. Eng., 2019, 7 (5), 103361. DOI: 10.1016/j.jece.2019.103361.

[28] LIU S., SHEN Y., WANG Y., SHEN P., XUAN D., GUAN X., SHI C., *Upcycling sintering red mud waste for novel superfine composite mineral admixture and CO_2 sequestration*, Cem. Concr. Comp., 2022, 129, 104497. DOI: 10.1016/j.cemconcomp.2022.104497.

[29] WANG D., FANG Y., ZHANG Y., CHANG J., *Changes in mineral composition, growth of calcite crystal, and promotion of physico-chemical properties induced by carbonation of β-C_2S*, J. CO_2 Utiliz., 2019, 34, 149–162. DOI: 10.1016/j.jcou.2019.06.005.

[30] KIM M.S., JUN Y., LEE C., OH J.E., *Use of CaO as an activator for producing a price-competitive non-cement structural binder using ground granulated blast furnace slag*, Cem. Concr. Res., 2013, 54, 208–214. DOI: 10.1016/j.cemconres.2013.09.011.